EFFECTS OF IMPACT LOCATION AND ANGLE OF A FLYING CROSS BAR ON THE PROTECTION OF A LONG-ROD PENETRATOR

Yo-Han Yoo[1], Seung Hoon Paik[2], Jong-Bong Kim[3] and Hyunho Shin[4]
[1]*Agency for Defense Development, Yuseong, Daejeon 305-600, Republic of Korea*
[2]*Korea Institute of Construction & Transportation Technology Evaluation and Planning, Anyang, Gyeonggi-do 431-060, Republic of Korea*
[3]*Department of Mechanical and Automotive Engineering, Seoul National University of Science and Technology, Seoul, 139-743, Republic of Korea*
[4]*Department of Materials Engineering, Gangneung-Wonju National University, Gangneung, Gangwon-do 210-702, Republic of Korea*
E-mail: hshin@gwnu.ac.kr

Received October 2012, Accepted May 2013
No. 12-CSME-103, E.I.C. Accession 3423

ABSTRACT
Based on a finite element analysis, the performance of a flying cross bar in protecting a long-rod penetrator increases as the impact location moves toward the head of the penetrator. It also increases as the impact angle approaches right angle. The optimal impact location along the span direction of the bar varies depending on the bar diameter.

Keywords: flying cross bar; long-rod penetrator; depth of penetration; lateral disturbance.

CONCENTRATION ET ANGLE D'IMPACT D'UNE BARRE TRANVERSALE EN VOL ET LEURS EFFETS SUR LA PROTECTION D'UN PÉNÉTRATEUR LONGUE TIGE

RÉSUMÉ
Basé sur l'analyse des éléments finis, la performance d'une barre transversale en vol pour la protection d'un pénétrateur longue tige augmente à mesure que la concentration de l'impact se déplace vers la tête du pénétrateur. Elle augmente aussi à mesure que l'angle d'impact se rapproche de l'angle droit. La concentration optimale de l'impact le long de direction de la barre varie en fonction du diamètre de la barre.

Mots-clés : barre transversale en vol ; pénétrateur longue tige ; profondeur de la pénétration ; perturbation latérale.

1. INTRODUCTION

Current active armor technology is mainly based on the role of single or dual flying plates impacting an incoming long-rod penetrator [1–7]. The flying plate provides a lateral load to the penetrator, resulting in the change of flight direction, bending, rotation and/or breakage of the penetrator. However, plate types generally have low energy efficiency with respect to the input energy to fly the whole plate mass because only the small perforation area or mass encounters the penetrator while the rest of the plate mass is not used for protection. Flying a plate itself is never a simple task due to the excessive energy taken to fly the plate toward the incoming penetrator [8–10].

To overcome such demerit, various types of flying objects can be considered such as blocks, spheres, or a cross bar. The cross bar type possesses the merit of a higher probability of impacting the penetrator than spheres or blocks. Its feasibility to incapacitate the incoming long-rod penetrator was reported in [11]. In our previous work [12], the influence of some fundamental parameters such as the diameter and kinetic energy (velocity) of the bar on the performance of penetrator protection was numerically investigated under a limited condition where the impact takes place between the center of the penetrator and the center of the bar at a fixed impact obliquity of 45°. However, such scenario would be rare in a practical situation. The cases of impacts between other locations of the penetrator and other locations of the bar at other obliquities would be more probable.

As the small angle of yaw of the penetrator is known to significantly affect the subsequent depth of penetration in witness block [13], the changes in the impact location of the penetrator, that of the cross bar, and the angle of impact are expected to yield a significant change in the protection performance of the flying cross bar. In this sense, in the present numerical study, the effects of impact locations of the penetrator and the cross bar as well as the impact angle on the protection performance have been investigated systematically based on finite element analysis.

NUMERICAL ANALYSIS

A schematic view of the model is represented in Fig. 1 and the values of each parameter are listed in Table 1. Velocity of bar (in m/sec unit), V_b, at a given condition of $KE_b/KE_p = 1/8$ is shown in Table 2. Note that specifying the value of KEb/KEp is somewhat arbitrary because a higher KE_b/KE_p value will yield higher protection performance [12].

Only half of the three dimensional space was analyzed considering the symmetry of the model. If necessary, a full three dimensional computation has been carried out (the cases when the impact location of the cross bar is not center of the bar, i.e., the cases of $B = 0.1$ and 0.3). In order to maintain a similar mesh size for the penetrator, cross bar, and witness block, a fine mesh with the size of 0.67 mm (as compared to $D_p = 5$ mm) was used around the impact region of the witness block. A commercial finite element package (LS-DYNA) was used for the analysis. For space discretization, 8-node hexahedral solid elements with one-point integration [14] were used. Stress update scheme for elestoplastic material based on Jaumann stress rate was used [14]. For time integration, the central difference method was used with stability control [14]. The penalty method was used as contact-impact algorithm [14].

The penetrator is composed of tungsten heavy alloy DX2HCMF, and the cross bar and witness block are composed of steel (SIS 2541-03). The Johnson–Cook (JC) flow stress model [15] and the polynomial equation of state (EOS) were employed. The model formulation and parameters in the JC model and the polynomial EOS were shown in previous work [12].

Material erosion has been simulated by eliminating appropriate elements from the model during calculation when they reach a certain plastic strain limit. The empirical equivalent plastic strain limit of 1.5 is adopted in the current work based on a preliminary effort. No fracture models were considered for both the penetrator and the bar, and thus any failure of the material by the current simulation is purely caused

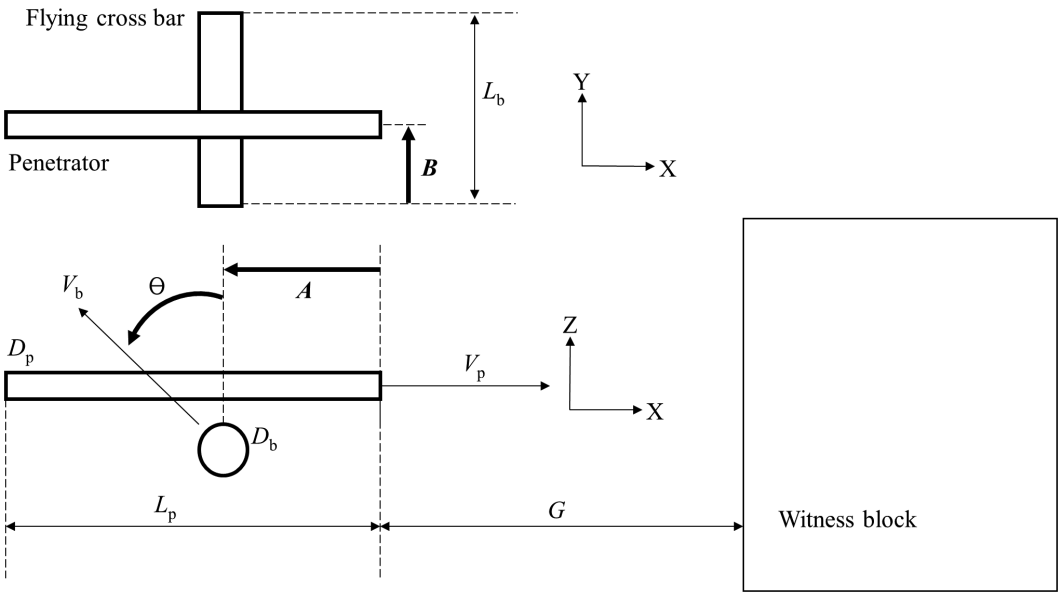

Fig. 1. Schematic view of the model. The top frame shows top view and the bottom frame side view.

Table 1. Design parameters for the impact of the cross bar to the long-rod penetrator.

Parameter	Symbol	Value
Length of penetrator	L_p	150 mm
Diameter of penetrator	D_p	5 mm ($L_p/D_p = 30$)
Velocity of penetrator	V_p	2 km/s
Length of the cross bar	L_b	75 mm
Diameter of cross bar	D_b	$D_b/D_p = 2, 4, 6$
Ratio of kinetic energy	KE_b/KE_p	1/8
Velocity of cross bar	V_b	Table 2
Distance of witness block	G	$4L_p$
Distance along the penetrator	A	0.25, 0.50, $0.75L_p$
Distance along the cross bar	B	0.1, 0.3, $0.5L_b$
Impact angle	θ	30°, 40°, 60°

Table 2. Velocity of bar (in m/sec unit), V_b, at a given condition of $KE_b/KE_p = 1/8$.

$D_b/D_p = 2$	$D_b/D_p = 4$	$D_b/D_p = 6$	$D_b/D_p = 8$
747.7	373.9	249.2	186.9

by the element erosion. As the tensile fracture with crack propagation is not replicated in the present work, actual performance could be different from the predicted results herein. Despite this limitation, the current numerical results may be used to examine the sensitivity of performance to design parameters, and in general, the trends, rather than absolute values, will probably be correct. The validity of adopting no fracture models together with the employed equivalent plastic strain limit (1.5) was checked in the previous work [12]. However, in the current work, the depth of penetration by the deformed penetrator after the interaction with the cross bar has a meaning on a comparative basis only between the simulation cases because of the lack of the tensile fracture mode of the penetrator.

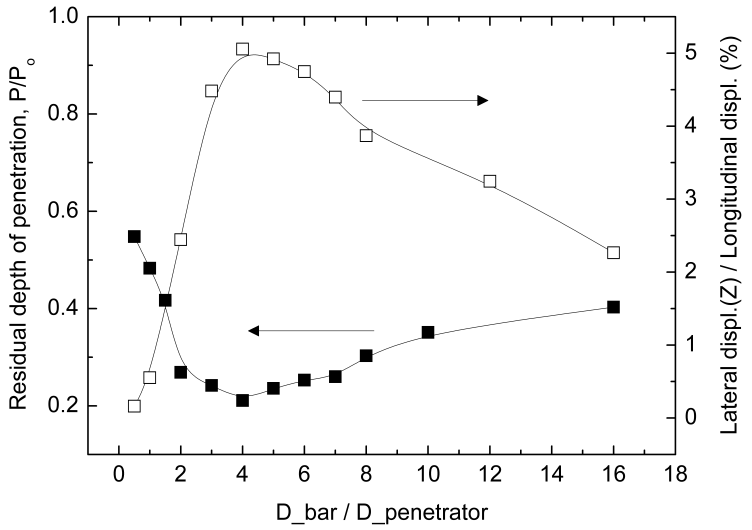

Fig. 2. Changes in the depth of penetration and lateral displacement as functions of D_b/D_p for the case when $\theta = 45°$, $A = 0.5L_p$, and $B = 0.5L_b$.

2. RESULTS AND DISCUSSIONS

2.1. Effect of the Diameter of the Cross Bar

The influence of the diameter of the cross bar on the protection performance has been investigated first for the case of the central impact ($\theta = 45°$, $A = 0.5L_p$, and $B = 0.5L_b$) prior to the investigation of the influences of impact location and angle. Figure 2 shows the effect of D_b/D_p on P/P_0, where P and P_0 are the depth of penetration in the witness block by the disturbed and undisturbed residual penetrators, respectively. Note that the velocity of bar (V_b) decreases with increased D_b/D_p since KE_b/KE_p is fixed to 1/8 in the present study (Table 2). In Fig. 2, the lateral displacement in the Z direction is normalized by longitudinal displacement of the penetrator just before it impacts the witness block. The lateral displacement (based on the movement of the center of mass) is a rigid body motion (rotation and translation) and the averaged deformation of the penetrator. The longitudinal displacement is $4L_p$ (= 600 mm). As shown in the figure, P/P_0 is minimal at around $D_b/D_p = 4$. The Z displacement is also maximal at this diameter, indicating that the lateral disturbance of the penetrator is highly correlated to the subsequent depth of penetration, and is an important mechanism in protection performance. Since the performance of the cross bar is maximal at around $D_b/D_p = 4$, the effects of impact location and impact angle of cross bar on the bar performance are examined hereinafter at varying D_b/D_p from 2 to 6.

2.2. Effect of Impact Location along the Longitudinal Direction of the Penetrator

The effect of impact location of cross bar in longitudinal direction of the penetrator on the resultant depth of penetration P/P_0 is shown in Fig. 3(a), for the case when $\theta = 45°$, $B = 0.5L_b$ ($A = xL_p$, $x = 0.25$, 0.50, and 0.75). The change in P/P_0 is plotted as a function of D_b/D_p from 2 to 6 as aforementioned for varying impact location, A. As the impact location moves from rear ($A = 0.75L_p$) to head ($A = 0.25L_p$) of the penetrator, a lower P/P_0 is observed. This decrease is due to the increased interaction time as the impact point moves toward head. While relatively small difference exists between $A = 0.25L_p$ and $0.5L_p$, when $A = 0.75L_p$, interaction time is insufficient, and thereby the P/P_0 value increases significantly compared with the case when $A = 0.50L_p$.

Note that when the impact location is near the head of the penetrator, e.g., when $A = 0.25L_p$, P/P_0 is not

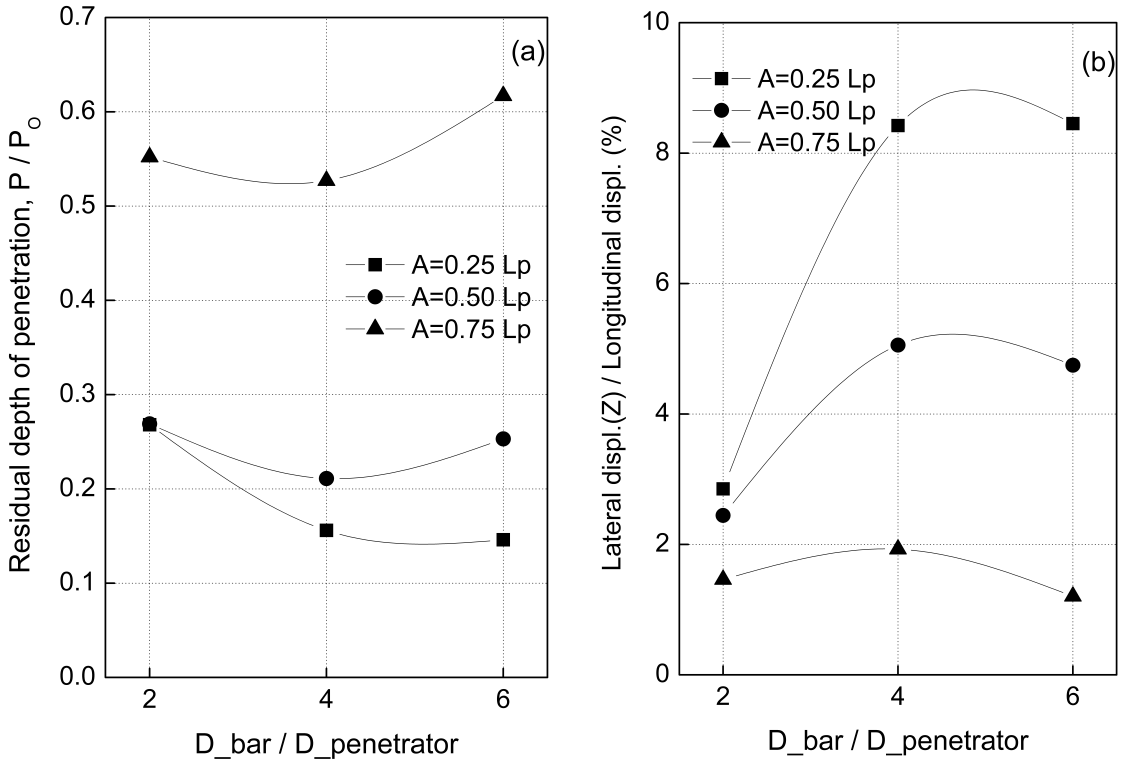

Fig. 3. Effect of impact location along the longitudinal direction of the penetrator on (a) the depth of penetration in witness block and (b) lateral displacement of the residual penetrator, for the case when $\theta = 45^\circ$ and $B = 0.5L_b$ ($A = xL_p$, x is varying as indicated in the figure).

minimum at $D_b/D_p = 4$, but keeps decreasing up to $D_b/D_p = 6$. In separate analysis, P/P_0 at $D_b/D_p = 8$ is lower than that at $D_b/D_p = 6$ (not shown). Thus, the D_b/D_p that yields the minimum P/P_0 when $A = 0.25L_p$ is expected to be higher or equal to $D_b/D_p = 8$. This finding indicates that a cross bar diameter thicker than $D_b/D_p = 4$ yields an improved bar performance, provided that the impact location is near the head of the penetrator.

Discussing the influence of impact location, A, on the lateral disturbance more in detail (Fig. 3b), a small difference in P/P_0 is observed at a small bar diameter, e.g., $D_b/D_p = 2$; however, this difference generally becomes larger as D_b/D_p increases. The lateral displacement increases as the impact point moves to the head of penetrator, which is consistent with the trend in P/P_0, indicating that it is a major mechanism to account for the observed trend in P/P_0.

In some impact conditions with the cross bar, the penetrator is broken with relatively sharp fracture surfaces [16], which is possibly due to the tensile fracture with crack propagation. As previously mentioned, the current simulation could not account for such fracture mode and thus any material failure is purely caused by the element erosion as mentioned previously. Nevertheless, the deformed shapes of the penetrator are presented in Figs. 4 and 5 for qualitative understanding of the interaction between the bar and the penetrator. In Fig. 4, deformed shapes of the penetrator after the bar impact and penetration process thereafter at varying time are shown for the case when $A = 0.5L_p$ and $D_b/D_p = 2$. Although the initial deformation of the penetrator shortly after the impact, e.g., 100 μs, is relatively small, the deformation augments and the whole residual penetrator rotates (rigid body rotation) thereafter until it reaches the witness block. Thus, a much larger entering crater forms as compared to the undisturbed penetrator. From the deformed shapes in Fig. 4, it seems that the deformation and rigid body rotation/translation of the residual penetrator are the major

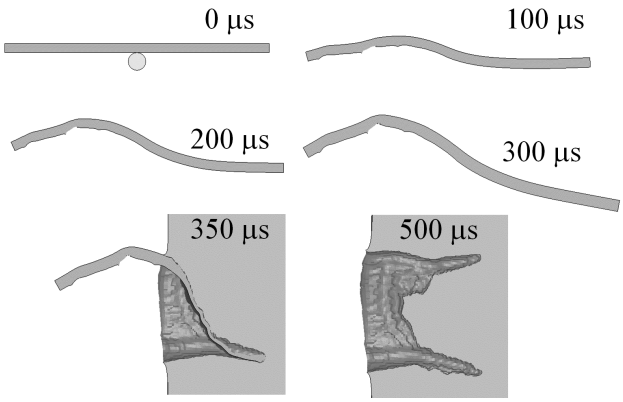

Fig. 4. Deformed shapes of the penetrator after bar impact and penetration process thereafter at varying time when $A = 0.5L_p$ and $D_b/D_p = 2$.

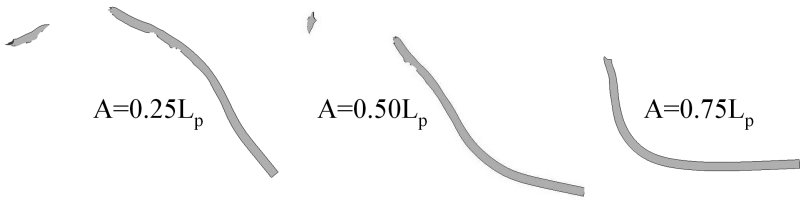

Fig. 5. Deformed shapes of the residual penetrator for varying impact location, A, along the longitudinal direction of the penetrator when time lapsed 300 μs after the bar impact ($D_b/D_p = 4$).

mechanism of interaction in light of the P/P_0 determined from the crater shape in the witness block; however, the erosion of the penetrator, especially on the impact side, does not appear to be an important defeat mechanism. Note that the deformed rear part of the penetrator forms another deep penetration hole in the witness block in addition to the one by the frontal part of the penetrator, which was not directly impacted by the cross bar, resulting in a 'C'-shaped crater.

The influence of the varying impact location A on the deformed shapes of residual penetrator is shown in Fig. 5 for the case when the cross bar diameter $D_b/D_p = 4$. The deformed shapes are taken at a time just before the arrival of the penetrator to the surface of the witness block (300 μs after the impact). As the impact location moves from rear ($A = 0.75L_p$) toward the head ($A = 0.25L_p$) of the penetrator, the deformed portion of the residual penetrator increases as the interaction time increases. Also, the rear part of the residual penetrator is even broken and the volume fraction of the broken rear part increases as the impact location moves toward the head. Such a mechanism of the breakage of the penetrator obviously assists the bar performance in reducing P/P_0.

2.3. Effect of Impact Location along the Span Direction of the Cross Bar

Now that the influence of the impact location along the longitudinal direction of the penetrator has been investigated, Fig. 6 presents the effect of impact location along the span direction of cross bar on P/P_0 and lateral displacement. Impact angle was 45° and the impact location along the longitudinal direction, A, was fixed to $0.5L_p$. Due to the offset of the cross bar, the model is now un-symmetric; thus, the analysis was performed with a full three dimensional model: the number of elements was twice the symmetric model.

As seen in Fig. 6(a), the P/P_0 is minimal again at $D_b/D_p = 4$, regardless of the impact location, B. When the diameter of the bar is large, e.g., $D_b/D_p = 6$, the performance of the bar is maximal when the impact

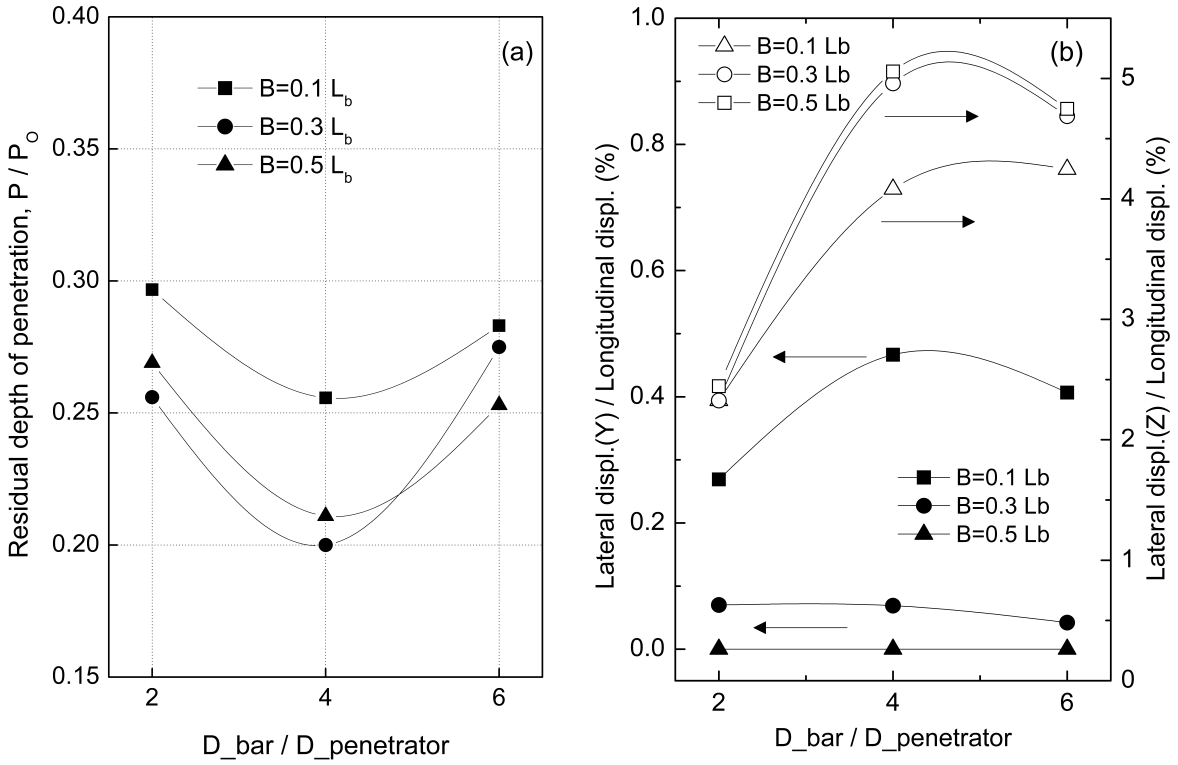

Fig. 6. Effect of impact location along the span direction of the penetrator on (a) depth of penetration in witness block, and (b) Y and Z displacement of the residual penetrator, for the case when $\theta = 45^\circ$ and $A = 0.5L_p$ ($B = xL_b$, x is varying as indicated in the figure).

takes place at the centre of the bar ($B = 0.5L_b$). However, interestingly, when the bar diameter is small, e.g., $D_b/D_p = 2$, and 4, it is no longer maximal at the centre of the bar, but rather at the impact location between the centre of the bar and edge, e.g., $B = 0.3L_b$, is more efficient in defeating the penetrator. The reason why the bar performance increases by the impact at off-centered position for the small bar diameters, e.g., $D_b/D_p = 2$ and 4, is because the rotation of the cross bar around the penetrator takes place due to the asymmetric impact of the cross bar. Indeed, the rotation of the cross bar would be more suitable if the diameter of the bar D_b/D_p is small, e.g., $D_b/D_p = 2$ and 4. The rotation of cross bar may yield the penetrator-erosion assisted reduction in P/P_0.

The optimum impact location along the span direction has to be pursued for varying D_b/D_p. However, an important point is that the influence of the impact location along the span direction, B, on the bar performance is far less apparent as compared to the influence along the longitudinal direction of the penetrator, A (Fig. 3a). This point is consistent with the small difference of the displacement (Fig. 6b) as B varies: only less than about 0.5 and 1% of the difference in lateral displacement along Y and Z directions, respectively. The improvement of the bar performance by impacting other positions than the centre of the bar is not apparent: the difference of P/P_0 value is only 0.05 when $D_b/D_p = 4$ and $B = 0.3L_b$ (Fig. 6a).

Top and side views of deformed shapes of the penetrator at 300 μs after the bar impact are presented in Fig. 7 for varying B. Deformed shapes of the cases when $B = 0.3L_b$ and $0.5L_b$ are more or less similar and the lateral displacements in Z-direction (side view) are higher than the case when $B = 0.1L_b$. Thus, the subsequent depth of penetration P/P_0 in the witness block (Fig. 6a) is similar for $B = 0.3L_b$ and $0.5L_b$ and is lower than the case when $B = 0.1L_b$.

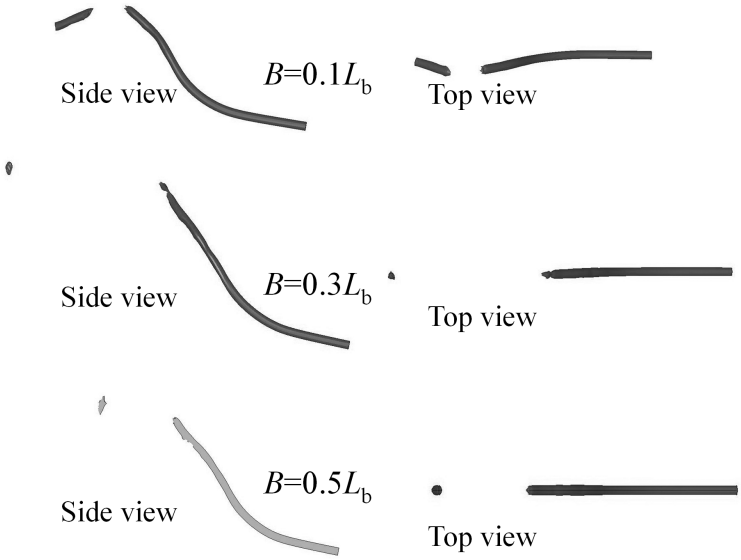

Fig. 7. Deformed shapes of the penetrator at varying impact location along the span direction, B (time = 300 μs; $D_b/D_p = 4$). Top and side views are defined in Fig. 1.

Note that in Fig. 7, no apparent difference exists in Y displacement (top view) for the impacts at $B = 0.1L_b$, $0.3L_b$, and $0.5L_b$. An interesting point is that when the location near the edge of the bar, e.g., $B = 0.1L_b$, impacts the penetrator (Fig. 7), increased volume of the rear part of the penetrator is broken away. In side view, the length of the main part of the penetrator is also decreased. As the impact near the edge of the cross bar induces an increased moment for the rotation of the cross bar, the breakage of the penetrator is suitably interpreted to be achieved because the rotation-induced erosion of the penetrator is localized in a smaller distance from the initial impact points. Also, the rotation of the cross bar well explains the increased Y deflection of the penetrator especially near the breakage area (top view of Fig. 7; $B = 0.1L_b$). For the cases of the impacts at $B = 0.3L_b$ and $0.5L_b$, which yield more symmetric impacts of the cross bar, rotation of the cross bar is diminished. Thus, the rotation-induced erosion place is spread along the penetrator length from the initial impact position, which may yield the smaller volume of the broken part of the penetrator. (Any eroded elements, which are not shown in Fig. 7 ($B = 0.3L_b$ and $0.5L_b$), may also assist to decrease the appeared volume of the broken rear part of the penetrator.)

Although the impact case at B=0.1Lb facilitates the early breakage of the penetrator as seen in Fig. 7, it results in an inferior protection performance of the bar as compared to the impacts at $B = 0.3L_b$ and $0.5L_b$ (Fig. 6a) because the Z displacement is smaller (Fig. 6b). This finding indicates that the Z-displacement is more important than the breakage of the penetrator (Fig. 7) or Y displacement (Fig. 6b) for the considered cases under the constraint of $A = 0.5L_p$. However, although the rotation of the cross bar is enhanced by varying B, the rotation (Z displacement) of the penetrator itself is negligible as compared to the impact cases with varying A. Thus, there exist only relatively small effects of offset B on the P/P_0 and Z displacement, as compared to the impact cases with varying A.

2.4. Effect of Impact Angle of the Flying Cross Bar

The effect of impact angle θ is shown in Fig. 8 for the case when $A = 0.5L_p$ and $B = 0.5L_b$. As θ decreases, P/P_0 becomes smaller, because the lateral displacement increases. Such increased protection performance with the decreased θ arises due to the increased interaction time. The minimum P/P_0 and the maximum displacement appears simultaneously at $D_b/D_p = 4$ for all of the angles considered here.

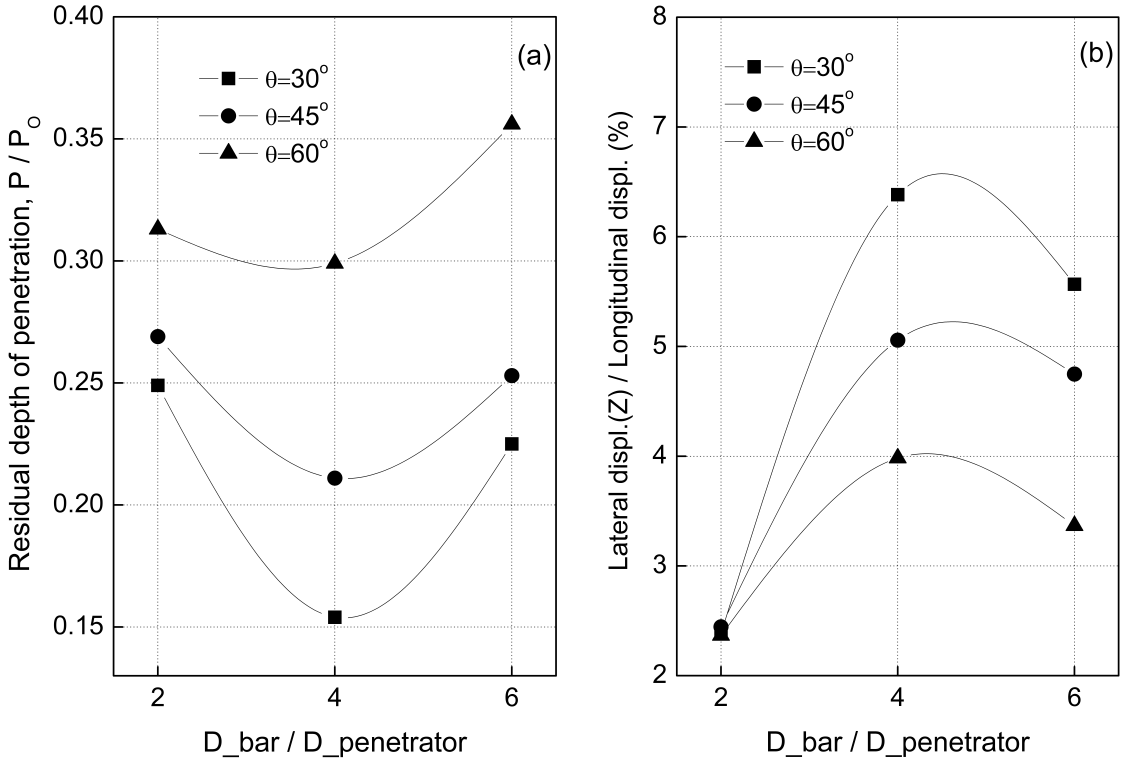

Fig. 8. Effect of impact angle on (a) the depth of penetration in witness block, and (b) Z displacement of the residual penetrator, for the case when $A = 0.5L_p$ and $B = 0.5L_b$ (θ is varying as indicated in the figure).

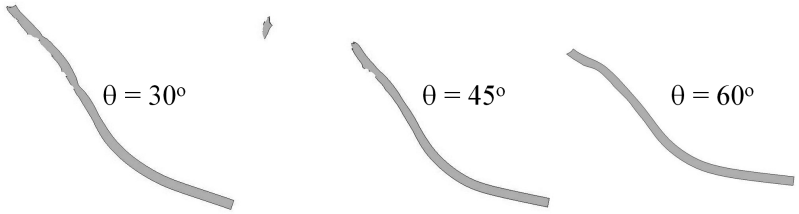

Fig. 9. Deformed shapes of the penetrator at 300 μs after the impact ($D_b/D_p = 4$; side view).

In Fig. 9, the deformed shapes of the penetrator is now shown depending on the impact angle $D_b/D_p = 4$. The deformed shapes were taken at 300 μs after the impact. As θ decreases, the lateral displacement in the rear portion of the penetrator is more pronounced and the rotation around the Y axis is more apparent, thereby improved protection performance is achieved as seen in Fig. 8(a).

3. CONCLUSIONS

Some design parameters of an active armor concept, which utilizes a flying cross bar instead of a flying plate, have been analyzed numerically. The influence of the impact location along the longitudinal direction of penetrator was investigated first. The kinetic energy of the bar KE_b was fixed to 1/8 of the penetrator KE_p.

The protection performance increases as the impact location moves toward the head of the penetrator. As for the influence of the impact location along the span direction of the cross bar, the impact location

yielding maximum bar performance varies depending on the bar diameter: impact at center is beneficial for a relatively large bar diameter; however, the location between the center and edge of the bar is better for a relatively small bar diameter, because the cross bar with a small diameter can more suitably rotate around the penetrator. Finally, a smaller impact angle toward the normal direction to the penetrator is beneficial in improving protection performance due to the increased interaction time.

The influence of impact location in the longitudinal direction of the penetrator is most pronounced among other effects, whereas the impact location along the span direction of the cross bar has a minimal influence on the performance of the cross bar. Lateral displacement associated with the rotation of the penetrator by the impact is a major mechanism in minimizing the depth of penetration in witness block.

ACKNOWLEDGEMENTS

This work was financially supported by the Basic Science Research Program through the National Research Foundation (NRF) of Korea, funded by the MEST (2010-0004150). It was also co-supported by the Gangneung Science Park Fosterage Program, funded by the Ministry of Education, Science and Technology of Korea through the Gangneung Science Industry Foundation (GSIF).

REFERENCES

1. Liden, E., Johansson, B. and Lundberg, B., "Effect of thin oblique moving plates on long rod projectiles: A reverse impact study", *International Journal of Impact Engineering*, Vol. 32, No. 10, pp. 1696–1720, 2006.
2. Shin, H. and Yoo, Y.-H., "Effect of the velocity of a single flying plate on the protection capability against obliquely impacting long rod penetrators", *Combustion Explosion and Shock Waves*, Vol. 39, No. 5, pp. 591–600, 2003.
3. Yoo, Y.-H. and Shin, H., "Protection capability of dual flying plates against obliquely impacting long rod penetrators", *International Journal of Impact Engineering*, Vol. 30, No. 1, pp. 55–68, 2004.
4. Paik, S.H., Kim S.-J., Yoo, Y.-H. and Lee, M., "Protection performance of dual flying oblique plate against yawed long rod", *International Journal of Impact Engineering*, Vol. 34, No. 8, pp. 1413–1422, 2007.
5. McIntosh, G. and Szymczak, M., "Ballistic protection possibilities for a light armoured vehicle", in *Proceedings of the 20th International Symposium on Ballistics*, Orlando, FL, USA, Vol. 2, pp. 1042–1048, September 23–27, 2002.
6. Sterzelmeier, K., Brommer, V. and Sinninger, L., "Active armor protection – Concept and design of steerable launcher systems fed by modular pulsed-power supply units", *IEEE Transactions on Magnetics*, Vol. 37, No. 1, Part 1, pp. 238–241, 2001.
7. Lee, W., Lee, H.-J. and Shin, H., "Ricochet of a tungsten heavy alloy long-rod projectile from deformable steel plates", *Journal of Physics, D: Applied Physics*, Vol. 35, No. 20, pp. 2676–2686, 2002.
8. Shin, H. and Lee, W., "Interactions of impact shock waves in a thin-walled explosive container, Part I: Impacts by a flat-ended projectile", *Combustion, Explosion, and Shock Waves*, Vol. 39, No. 4, pp. 470–478, 2003.
9. Shin, H. and Lee, W., "Interactions of impact shock waves in a thin-walled explosive container, Part II: Impact by a cone-nosed projectile", *Combustion, Explosion, and Shock Waves*, Vol. 39, No. 4, pp. 479–486, 2003.
10. Shin, H. and Lee, W., "Material design guidelines for explosive confinements to control impact shock-induced detonations based on shock transmission/reflection analysis", *International Journal of Impact Engineering*, Vol. 28, No. 5, pp. 465–478, 2003.
11. Liden, E., Andersson, O. and Tjernberg, A., "Influence of side-impacting dynamic armour components on long rod projectiles", in *Proceedings of the 23rd International Symposium on Ballistics*, Tarragona, Spain, Vol. 2, pp. 1099–1106, April 16–20, 2007.
12. Yoo, Y.-H., Paik, S.H., Kim, J.-B. and Shin, H., "Performance of a flying cross bar to incapacitate a long-rod penetrator", *Engineering with Computers*, Vol. 39, No. 4, pp. 409–415, 2013.
13. Gee, D.J. and Littlefield, D.L., "Yaw impact of rod projectiles", *International Journal of Impact Engineering*, Vol. 26, No. 1–10, pp. 211–220, 2011.
14. Hallquist, J.O., *LS-DYNA Theory Manual, Livermore Software Technology Corporation*, Livermore, CA, USA, 2006.

15. Johnson, G.R. and Cook, W.H., "A constitutive model and data for metals subjected to large strains, high strain rated, and high temperatures", in *Proceedings of the 7th International Symposium on Ballistics*, The Hague, The Netherlands, pp. 541–547, April 19–21, 1983.
16. Liden, E., Ottosson, J. and Holmberg, L., "WHA long rods penetrating stationary and moving oblique steel plates", in *Proceedings of the 16th International Symposium on Ballistics*, San Francisco, CA, USA, Vol. 2, pp. 703–711, September 23–28, 1996.
17. Anderson Jr., C.E., Walker, J.D., Parton, S.J. and Bless, Y., "On the L/D effect for long-rod penetrators", *International Journal of Impact Engineering*, Vol. 18, No. 3, pp. 247–264, 1996.
18. Anderson Jr., C. E., Walker, J.D., Bless, S.J. and Sharron, T.R., "On the velocity dependence of the L/D effect for long-rod penetrators", *International Journal of Impact Engineering*, Vol. 17, No. 1–3, pp. 13–24, 1995.